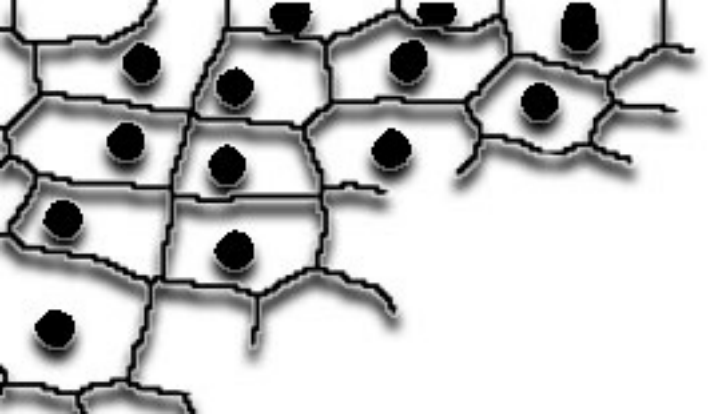

6

The Protein-Tyrosine Phosphatase Family in Gastrulation Cell Movements in Zebrafish

Vincent Runtuwene, Mark van Eekelen and Jeroen den Hertog

Abstract

The zebrafish model ideally lends itself to large scale morpholino screens due to its high fecundity and ease of morpholino injection. Moreover, zebrafish embryos are optically transparant, facilitating morphological analysis of developmental defects. We took advantage of the zebrafish system to screen the entire family of classical protein-tyrosine phosphatases. Despite the fact that this family of proteins has been studied intensively, still relatively little is known about its function *in vivo*. We designed 2 splice site morpholinos for each of the 48 genes, encoding protein-tyrosine phosphatases. In the first round all embryos were analyzed morphologically, which resulted in the identification of four candidate genes with a potential role in convergence and extension. These positive hits were analyzed in detail for convergence and extension defects in the second round by *in situ* hybridization and confocal microscopy-based cell shape analysis, yielding one *bona fide* novel PTP with a role in convergence and extension cell movements.

Introduction

Reversible tyrosine phosphorylation of proteins is a key mechanism for transducing inter- and intracellular stimuli, and acts as a highly dynamic molecular switch between different activation states of signaling molecules [1-3]. Given its elemental role it is not surprising that disruption of the synergy between protein-tyrosine kinases (PTKs) and phosphatases (PTPs) underlies many human diseases and developmental defects [4-9]. While much work has been done in the characterization of PTKs, the function of many PTPs remains to be elucidated.

During gastrulation, the zebrafish morphology undergoes a drastic change from an apparent homogeneous, 'inverted cup'- shape to a bilaterally symmetric, narrow and long body frame. This impressive remodeling is due in great part to the evolutionary conserved convergence and extension (CE) cell movements [10]. Together with epiboly and internalization, the CE movements form the germ layers, ectoderm, mesoderm and endoderm. Additionally, they are crucial for proper organ anlage positioning and as a consequence are essential for normal development [11]. Collective polarization of the cells in the mediolateral direction is essential for both the convergence towards the midline as well as intercalation, which is needed for extension in the anterio-posterior direction. Cell polarization is in part regulated by the non-canonical Wnt/PCP pathway [12-15]. Cell adhesion has also been implied to be a key factor in zebrafish CE movements [16].

We are interested in the role of PTPs in CE cell movements. Previously, we have identified all members of the family of classical PTPs in the zebrafish genome and provided a detailed analysis of the spatio-temporal expression patterns of these 48 PTPs during early embryonic development. Many PTPs are maternally contributed and most PTPs are ubiquitously expressed at shield stage [17]. We and others have shown that knockdown or knockout of several members of the family of classical PTPs, including *ptpra*, *ptprea*, *ptpreb*, *ptpn11*, and *ptprua* affect the CE cell movements during zebrafish gastrulation [18-20]. Moreover, we have recently found that *ptpn13* and *ptpn20* are required for normal gastrulation cell movements as well (Chapter 3, this thesis). These morphant and mutant embryos show a common shorter and broader phenotype. For *ptprea* and *ptpreb*, simultaneous knockdown was necessary to produce a phenotype, suggesting redundant functions of these ohnologs [19]. Given the role of some PTPs in CE cell movements and given that the majority of transmembrane PTPs encode components of cell adhesion molecules in their extracellular domain, including immunoglobulin-like domains and Fibronectin type III repeats, which may mediate cell-cell contacts and thus play a role in CE cell movements during gastrulation, we were interested to investigate the function of all classical PTPs in CE.

We set out to perform a functional screen on the role of the entire family of classical PTPs in gastrulation CE movements, using morpholino (MO) based gene knockdown. For each PTP, two independent splice site MOs were used. Initially, knockdown was assessed on a morphological basis. A gene was considered positive when both MOs generated a significant reduction in tail length at 72 hpf. In total 41 PTPs with unknown function in CE movements were analyzed and four of these genes were considered to be positive based on this principle. In the second round, the four positives were scored more directly for defects in CE movements using two independent methods: *in situ* hybridization with CE specific probes and analysis of the polarization of the presomitic mesoderm using confocal microscopy. Based on these tests, we found that one of these genes had a role in CE cell movements, namely *ptprda*. To our knowledge this is the first MO screen in which an entire protein family was systematically knocked down.

Results

Screening for PTPs that affect CE cell movements

In the present study we aim to identify PTPs which have a role in CE movements during gastrulation. Previously, we have identified all members of the classical PTP family in the zebrafish genome. Here, we designed a functional screen to assess the role of each PTP in early development (Fig. 1). Briefly, we designed two independent splice site MOs for all PTPs. Each MO was injected into zebrafish embryos at the one-cell stage and phenotypes were assessed at 24, 48 and 72 h post fertilization (hpf). Embryos with shorter body axis were selected and the tail length was determined at 72 hpf as a first indication of potential CE cell movement defects. Subsequently, p53-MO was co-injected with each of the PTP-MOs to rule out that the observed defects were caused by non-specific p53-dependent DNA damage responses. Finally, candidate hits where the two MOs induced similar developmental defects in a p53-independent manner were selected and subjected to specific analysis of defects in CE cell movements.

Design of the MOs

Using the previously identified PTP sequences in the almost completely sequenced zebrafish genome, version Zv8, we designed splice site MOs [17, 22]. Several human PTP encoding genes like *PTPRC*, *PTPRD*, *PTPRE*, *PTPRS*, *PTPRF* and *PTPRO* have been shown to generate multiple isoforms, usually differing in the N-terminal extracellular domain in receptor-like PTPs, which are assumed to be formed by alternative splicing [23-25]. Yet, expression of PTPRE and PTPRO isoforms is driven by alternative promoters, resulting in transmembranal and cytosolic isoforms, respectively [26, 27]. It is highly likely that other PTP genes

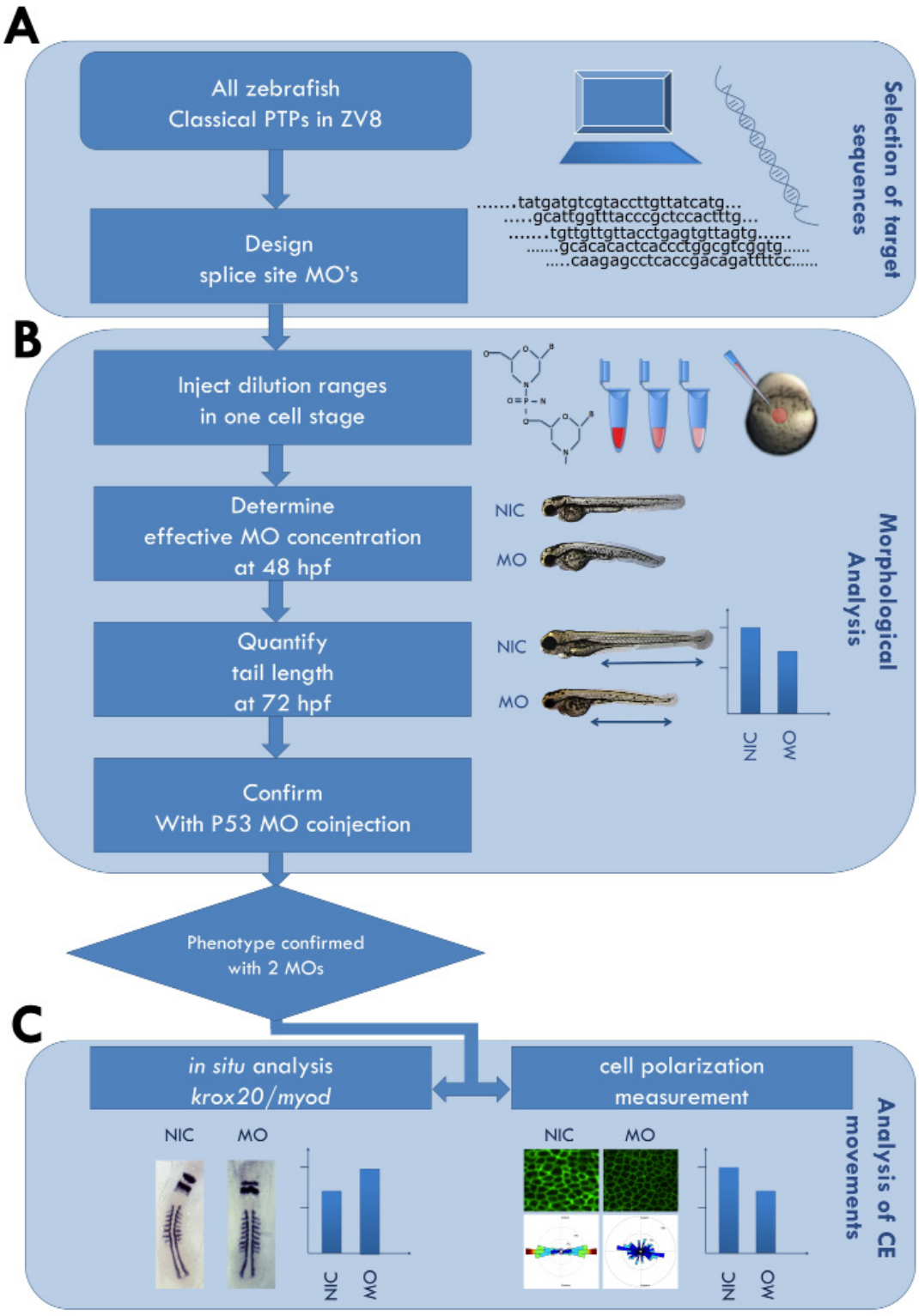
A
All zebrafish
Classical PTPs in ZV8
Design
splice site MO's
.....tatgatgtcgtaccttgttatcatg...
.....gcattggtttacccgctccactttg...
.....tgttgttgttacctgagtgttagtg.....
.....gcacacactcaccctggcgtcggtg.....
.....caagagcctcaccgacagattttcc.....
Selection of target sequences
B
Inject dilution ranges
in one cell stage
Determine
effective MO concentration
at 48 hpf
Quantify
tail length
at 72 hpf
Confirm
With P53 MO coinjection
NIC
MO
NIC
MO
NIC
MO
Morphological Analysis
Phenotype confirmed
with 2 MOs
C
in situ analysis
krox20/myod
cell polarization
measurement
NIC
MO
NIC
MO
NIC
MO
NIC
MO
Analysis of CE movements

Figure 1. Schematic overview of the screen for PTPs with a role in CE movements.
(A) Splice site MOs were designed based on the identified PTP sequences in the zebrafish genome (version ZV8). (B) Dilution ranges of MOs (0.3 – 5.0 ng/nl) were injected to determine an efficient MO concentration, defined as the lowest concentration that induced morphological defects at 48 hpf. The tail lengths of embryos were quantified at 72 hpf. The embryo phenotypes were confirmed by coinjection of p53 MO. (C) When 2 MOs cause a significant reduction in taillength and both are confirmed by coinjection of p53 MO, we proceeded with quantitative tests for the analysis of specific aspects of CE. In situ hybridization was done with well characterized markers for CE movements. Analysis of cell polarity in the presomitic mesoderm was done by confocal microscopy and automated scoring of cell shape.

generate different isoforms through similar mechanisms. The use of ATG MOs would only suppress the expression of certain isoforms of a PTP gene. Therefore, we designed splice site MOs targeted at the exon-intron boundaries within the PTP domain, immediately upstream of the catalytic site to ensure that the MOs disrupt the phosphatase activity of all isoforms of the respective PTPs. For all PTP genes, two splice site MOs (25-mers) were designed in accordance with the criteria provided by the manufacturer (http://www.gene-tools.com/) (Table 1).

Gene	MO name	sequence
ptprc	MO1*	ACAAAGCACAAACCTTATTTCCTTC
	MO2	CCCTATCTGTACCTGCAGTGGACCA
ptprm	MO1*	TTGATGCTGCACCTTCTCCACAGCG
	MO2	ATTCTCCTGTACCTGCAGTGCACCA
ptprk	MO1*	AAAATAATCTCACCCTCTCCAGAGT
	MO2	GGCCACACACACCTCGGTCTGTACC
ptprt	MO1	AAAGAGATTTTACCTTCTGTACAGT
	MO2	ATAGCAGCATACCTGCAGTGAACCA
ptprua	MO1*	AGTCATCTCGTACCCGCTCCAGGGC
	MO2*	GAAGCTCCATACCTGCAGTGCACCA
ptprub	MO1	TAACACACTTACCCGCTCCATGGCA
	MO2	AGTAATTTCTACCTGCAGTGGACAA
ptprfa	MO1	GGAACTTTTTACCTTGTAAAGGGCA
	MO2*	AACCGTACTCACCTGCAGTGCACTA
ptprfb	MO1*	GAACACACACACCTTGTAGAGAGCG
	MO2	GTCACGCTGTACCTGCAGTGCACCA
ptprsa	MO1	TTGAAATCTTACCTTGTGCAAGGAG

	MO2	CAGATTTCAGACCTGCAGTGGGCGA
ptprsb	MO1*	GCACACACTCACCCTGGCGTCGGTG
	MO2*	GTCGTGTTTTACCTCAGTCTGCACC
ptprda	MO1*	CTGTTTGGTTACCTTAAAGAGGGCA
	MO2*	GGTAATAGCTACCTGCAGTGGACCA
ptprdb	MO1	CACCGCTCGTACCCTGGACCGCTCC
	MO2	TGAGAGTCAGACCTGCAGTGCACCA
ptprb	MO1	GACTCCACTTACGCATGATATTTTG
	MO2	TGTGACTCTTACCTCGGTTTGTACC
ptprja	MO1	TGAGGTTCTTACATGGCAGCACATT
	MO2	TGAGGTTCTTACATGGCAGCACATT
ptprh	MO1	ACATTGCCTTACCCTTCCACCCTCA
	MO2	GAAATGGCTTACATTTTTGACATTA
ptprq	MO1	GCATTGGTTTACCCGCTCCACTTTG
	MO2	GCGTCTGTGTACCTGCAGTGGACCA
ptpro	MO1*	TGTTTTCCTCACGTATGCGAGTCTG
	MO2*	GTTAGCACTGACCCTGCGGCGCTCG
ptpra	MO1*	TTGCGGCGTTTACCTCTTTCCGCTC
	MO2*	TGCCCTGGAGAAACGAAACCTGCAT
ptprea	MO1*	AAGGGATGCTAACCTCTTTTCTCTC
	MO2*	ATTAAGACTTACATATTGCACACAG
ptpreb	MO1*	TATCTTATCTCACCTCTTTTCTCTC
	MO2*	CTGCAGTCTTACCTACAGTGCACTA
ptprga	MO1	AAACATTGTGTACCTTCTTTACTTT
	MO2	TGTGGGTTTTACCTGCAGTGTACAA
ptprgb	MO1*	ATGGATACTCACCCTGCCTTTCTCC
	MO2*	GCTTTAACGCACCTTTTTCAGTTTG
ptprza	MO1*	CTCAAAGCCTTACCCGGCCCTTCTC
	MO2	GTAACTGCTTACCTGCAGTGCACCA
ptprzb	MO1	AAAATGTCTTACCCTTCCTTTCTCC
	MO2	AAATATTGATACCTTTTTTATGCTG
ptprr	MO1	ATCAGGACTTACTCGTATGTAGTTG
	MO2*	TCAGATACTGACTTGGCAAAATGGT
ptprna	MO1	GGTTTTCAGTAGGTGCGGAAGTCCA
	MO2	AAGTTTGCTTACCTTTGGCCATGCG
ptprnb	MO1	ATGTATGCAGTACCTGCGAAAGTCC
	MO2	TGAAGTGCTGACCTTTAGCCATGCG

ptprn2	MO1	TGTGGACACATACCTGCGGAAGTCC
	MO2*	TGTGGTACTTGCCTGCAATGAACAA
ptpn1	MO1	CAAGAGCCTCACCGACAGATTTTCC
	MO2	CCGTCATCTCACCAATAGAAGGCAG
ptpn2	MO1*	AATGTGACTCACCGTGCCTTTCTCT
	MO2	TTACATTCACACCTTGCCATTTTGA
ptpn6	MO1	ACTCATTCCTTACCCGATGCGGAGC
	MO2*	TTATTAAAGTACCTGCAGTGAATGA
ptpn11a	MO1*	GAAACCCTTTACCTTTCCCCGTTCC
	MO2*	GGTGGAACCACCTTCGGGATGTCAT
ptpn11b	MO1	GCATTGCTCTTACCCTGTCTAGACG
	MO2	CCTGGACCTTACCCGTCCTCTCTCC
ptpn9a	MO1	TATGATGTCGTACCTTGTTATCATG
	MO2	TTAGAAATGTACCTCAGTGTTGTGC
ptpn9b	MO1	TAACGAAACTAACCTTGTAGTCATA
	MO2*	TAAGAAACTAACCTGAGTGTTGAAC
ptpn18	MO1	TGAAACAGCTCACCTTAACATTATG
	MO2	GAAAACACTTACAGTTGAGACAGTA
ptpn3	MO1	TGTTGTTGTTACCTGAGTGTTAGTG
	MO2*	ACGAAGTTGTACCGATGTCTGAACC
ptpn4a	MO1	GTGATAAGCTCACCTCAATGTGAGT
	MO2	ATGTGGACTTACAGGCGTCTGAATC
ptpn4b	MO1*	ATGCTTTTCATACCCGGCCCCGCTC
	MO2	TCCAGGCCTGACCTGCAGTGAACCA
ptpn21	MO1	GTGCTGTACTTACAGAGAAAGCCTT
	MO2*	TGCAGTGCATACCTCATTGTGTTCC
ptpn13	MO1*	CTCTCTCTCTCACCTGGACGTCTTT
	MO2*	TGTGACACTTACATCTGCGTCTTTG
ptpn23a	MO1	AAAAGTCCCTTACAGTTCAGGCCAT
	MO2	TAAGTGGTTTACCTTTAGTGTAATG
ptpn20	MO1*	CATGCTCCTAACCTTTTTTTCCACC
	MO2	TAAATGACTCACACTGAGGTCTTTC
ptpn5	MO1	AACTCAGACAGACCTTCACAGTGAA
	MO2*	TAAAAATGTTACCTGCAGTGGACGA

Table 1. PTP genes and Morpholino sequences.
All splice site MOs were designed to target one (marked MO1) or two (marked MO2) exons upstream of the catalytic site and manufactured by Genetools (Pilomath, OR, USA). MOs, that caused a CE defect based on morphological analysis are marked with an asterisk (*).

PTP-MO induced tail length defects

Gene knockdown was achieved by injection of MOs at the one cell stage. In at least two independent experiments we injected dilution ranges from 0.3 to 5.0 ng/nl per embryo, using 50 embryos per condition (n= 50). Effective concentrations for each MO were determined as the lowest concentration at which defects in morphology were clearly visible at 48 hpf in at least 80% of the injected embryos (Fig. 2A). As a quantitative read-out for body axis extension, a hallmark of CE defects, we determined the tail length at 72 hpf (Fig. 2B). A hit was considered positive when both MOs generated a significant reduction in tail length at 72 hpf. Of 41 PTPs with unknown function in convergence and extension movements, four genes were considered to be positive based on these criteria: *ptprsb*, *ptprda*, *ptpro* and *ptprgb*. As positive controls, we included *ptprua*, *ptpra* and *ptprea/b* (combined *ptprea* and *ptpreb*) that are known to have a role in CE cell movements. Genes of which only one MO caused a significant reduction in tail length were considered tentatively negative and were excluded from further analysis.

Previous studies reported a shortened AP-axis, neural toxicity, widespread cell death, and defects in epiboly as possible off-target or non-specific effects [28-30]. The risk of observing these effects increases significantly when using MO concentrations higher than 5 ng/nl [31-33]. Indeed, in our hands neural toxicity, cell death, defects in epiboly, and shortened AP-axes were occasionally observed upon injection of high concentrations of MO. However, for all four positive hits effective MO concentrations were below 5 ng/nl. Furthermore, the replication of the phenotype using a second sequence-independent MO, reduces the probability that the observed phenotype is an off-target effect to great extent and in fact two independent morpholinos are considered as the standard for MO specificity. To ascertain that the observed phenotypes were not caused by a mere non-specific DNA damage response, all hits that were positive for both MOs were subsequently coinjected with a p53-specific MO, which has been shown to alleviate non-specific MO phenotypes by blocking p53-dependent apoptosis [34]. None of the four positive hits were affected by co-injection of p53-MO. Whereas all four candidate genes caused a reduction in tail length, the knockdowns induced clearly different overall morphological defects (Fig. 2A), warranting specific analysis of the effects on CE cell movements in response to knockdown of these four PTPs.

Analysis of CE movements

CE cell movements during gastrulation are characterized by mesendodermal cells that migrate towards the dorsal midline, intercalate and consequently contribute to body axis extension. These critical cellular rearrangements are largely driven by highly coordinated shape changes, *i.e.* collective polarization and elongation in the mediolateral direction [11]. Therefore, overall CE cell move-

ment defects are characterized by shorter and broader embryos. At the cellular level, CE cell movement defects are characterized by defective polarization, reduced cell elongation and defective cell orientation.

To investigate whether the shortened body axis was caused by defective CE cell movements, we performed *in situ* hybridization experiments on embryos fixed at 8-10 somite stage using the *krox20* and *myod* probes, well-established markers for CE cell movements [19, 35, 36] (Fig. 3A). The *krox20* probe stains rhombomeres 3 and 5. The width of these structures is used as a measurement for convergence. The *myod* probe stains the somites. The distance from the first to the eighth somite is used to analyze extension. Defects in CE movements will cause a wider *krox20* staining and a shorter distance between the first and eighth

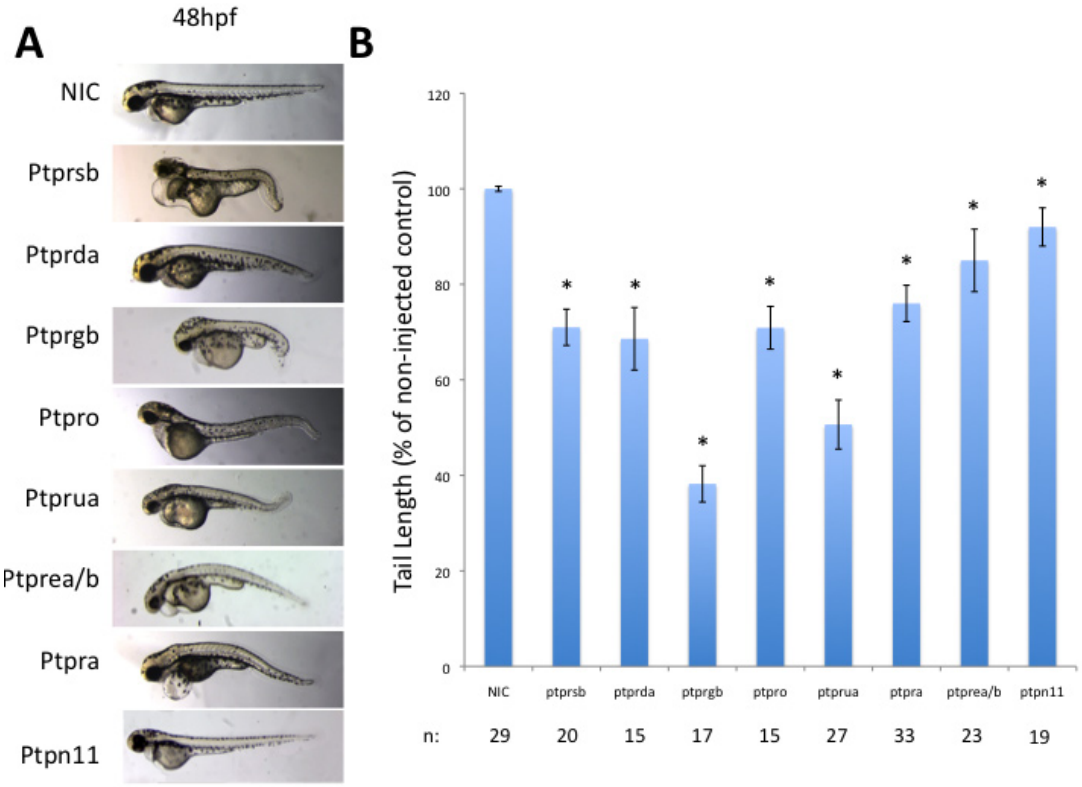

Figure 2. Knockdown of Ptps causes a shorter anterio-posterior axis.
(A) Representative phenotypes at 48 hpf after injection at 1-cell stage with a MO targeting *ptprsb* (1,25 ng), *ptprda* (1,25 ng), *ptprgb* (1,25 ng), *ptpro* (1 ng) *ptprua* (1,25 ng), *ptpra* (0,3 ng), *ptprea/b* (mix of 2,5 ng *ptprea* and 2.5 ng *ptpreb*), *ptpra* (0,3 ng) or *ptpn11* (1 ng). Injections were done at least twice for each MO. (B) Quantification of the phenotypes shown in panel (A). Individual tail lengths, i.e. the distance between the beginning of the yolk extension and the tip of the tail, of embryos at 72 hpf from each group were measured using ImageJ software and the data were analyzed statistically in excel using a 2-tailed student t-test assuming unequal variances. Significant differences were determined using a=0,05 upon comparison to the ratio of the non-injected control (NIC). Significant differences are indicated with an asterisk.

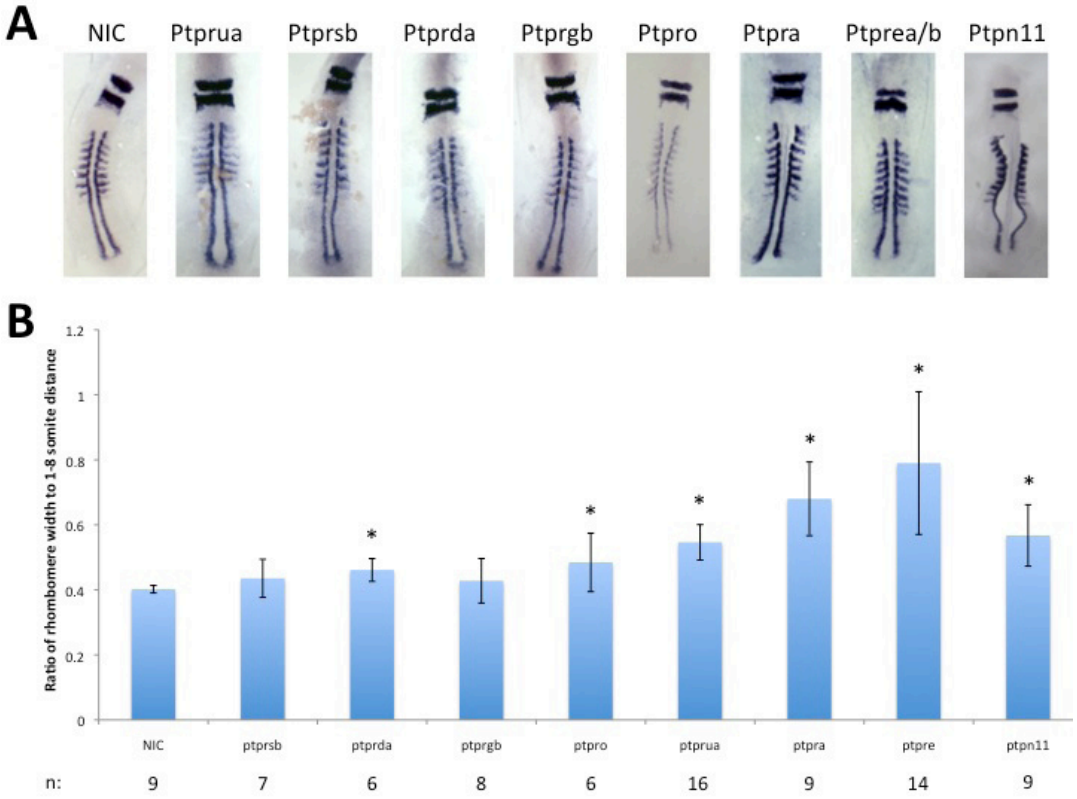

Figure 3. CE defects in PTP knockdowns.
(A) Embryos were injected at 1-cell stage with a MO targeting *ptprua* (1,25 ng), *ptprsb* (1,25 ng), *ptprda* (1,25 ng), *ptprgb* (0,625 ng), *ptpro* (1 ng) *ptpra* (0,3 ng), *ptprea/b* (mix of 2,5 ng *ptprea* and 2,5 ng *ptpreb*), and *ptpn11* (1 ng). The embryos were fixed at the 8-10 somite stage and in situ hybridisation was done using *krox20*- and *myod*-specific probes. The *krox20* probe stains rhombomere 3 and 5 and the *myod* probe stains the somites. The ratio between the width of the rhombomeres and the distance between the 1st and 8th somite was determined as a direct measure for CE cell movements. A representative embryo from each group is shown. (B) The resulting ratios for all MOs from (A). The data was statistically analyzed in excel using a 2-tailed student t-test assuming unequal variances. Significant differences were determined using a=0,05 upon comparison to the ratio of the non-injected control. Significant differences are indicated with an asterisk.

somite. Defects can readily be quantified by comparing the ratio of rhombomere width to somite distance between MO injected embryos and NIC embryos (Fig. 3B). Knockdowns of PTPs with a known role in CE cell movement defects resulted in a significant increase in this ratio for each of these genes (Fig. 3B). *Krox20/myod in situ* patterns showed that knockdown of *ptprda* and *ptpro* caused a significant increase of the rhombomere width to somite distance ratio at 8-10 somite stage, in contrast to *ptprsb* or *ptprgb* (Fig. 3B).

To asses defects in cell polarization, we determined the elongation and polarization angle of the presomitic mesendodermal cells. We used confocal micros-

copy to visualize the cellular membranes in the presomitic mesoderm at the 2 to 3 somite stage. In order to fluorescently mark the membranes, the embryos were injected with 20 pg of YFP-CAAX mRNA. The presomitic mesoderm was imaged 100 µm posterior to the developing somites in the paraxial mesoderm, lateral to the notochord. All cells within a region of 14000 μm^2 were analyzed in each sample by an automated algorithm. In order to get a more machine-interpretable representation of the cell shapes, we used a custom-made ImageJ plug-in, Cell Outliner, to convert the raw confocal images to binary representations, wherein the fluorescent membranes were segmented into a model with uniform intensity and line thickness (Chapter 5, this thesis). This was necessary because the inherent fluctuation in fluorescence intensity in raw confocal images causes artefacts. Subsequently, the cell shapes were analyzed regarding aspect ratios of length and width, i.e. cell elongation, and orientation of the long axis in relation to the mediolateral direction, i.e. cell polarization angle. Further, using an adapted windrose plug-in in Matlab, radial color-coded histograms were made showing the relationship between the distribution of the cell polarization angle and cell elongation, henceforth referred to as Cell Roses (Fig. 4A) (Chapter 5, this thesis). Additionally, the cell aspect ratios were compared separately between MO injected embryos and NIC (Fig. 4B). Using this method we observed for *ptpra*, *ptprea/b*,

Figure 4. *Ptprda* is required for normal gastrulation cell movements.
(A) Embryos were injected at 1-cell stage with a MO targeting *ptprua* (1,25 ng), *ptprsb* (1,25 ng), *ptprda* (1,25 ng), *ptprgb* (1,25 ng), *ptpro* (1 ng) *ptpra* (0,3 ng), *ptprea/b* (mix of 2,5 ng *ptprea* MO and 2,5 ng *ptpreb* MO), and *ptpn11* (1 ng). All embryos were coinjected with YFP-CAAX mRNA (25 pg) a fluorescent marker for the cell membranes. The embryos were mounted at shield stage on the dorsal side, approximately 100 µm posterior to shield position. (A) Imaging of the presomitic mesoderm was performed at 2-3 somite stage. The cell shape segmentation was performed using a custom made plugin, Cell Outliner, in ImageJ and the resulting data was plotted using a Cell Rose (an adapted windrose plot plugin in Matlab). ImageJ determines the angles of the major axes of the cells within the PSM to the notochord (the orientation of the notochord is parallel to the vertical axis, marked on top "anterior" and at the bottom "posterior"). In addition, ImageJ measures the length to width ratios of the cells. The graphs in (A) show the distribution of the orientations of the cells in the presomitic mesoderm in radial histograms. Two circles on the graphs represent the 5% (inner circle) and 10% (outer circle) population fraction markers for the radial histogram. Within the bars of the histogram, a second subdivision is shown, indicating the frequencies (by surface area) and intensity of elongation (aspect ratio is indicated in colour code as indicated in the legend, bottom right) of cells within that particular population. Student-t statistics was used to compare the cell elongation values and Watson U2 statistic was used to compare the orientation data of the cells. As such, the resulting Matlab windrose graphs in (A) show both the polar distribution of all cell angles and shows in color code (see legend) the extent of polarization of the cells within a certain orientation. Statistical comparison data displayed, resulted from comparison of a MO-injected embryos to NIC siblings within the same experiment. (B) Bar graph of the polarization of the PSM solely based on the major/minor axes ratios. The data was statistically analyzed in excel using a 2-tailed student t-test assuming unequal variances. Significant differences were determined using a=0,05 upon comparison to the ratio of the non-injected control. Significant differences are indicated with an asterisk.

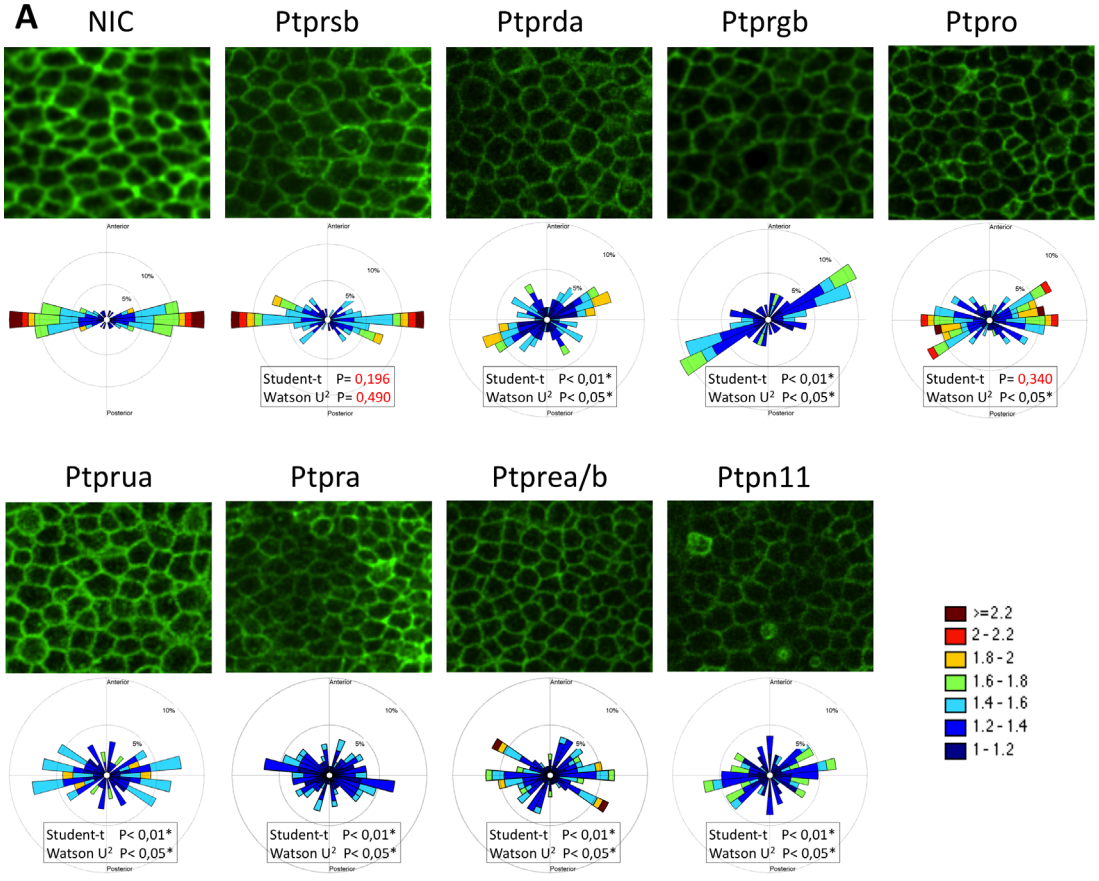
A
NIC
Ptprsb
Ptprda
Ptprgb
Ptpro
Ptprua
Ptpra
Ptprea/b
Ptpn11
Student-t P= 0,196
Watson U² P= 0,490
Student-t P< 0,01*
Watson U² P< 0,05*
Student-t P= 0,340
Watson U² P< 0,05*
>=2.2
2 - 2.2
1.8 - 2
1.6 - 1.8
1.4 - 1.6
1.2 - 1.4
1 - 1.2

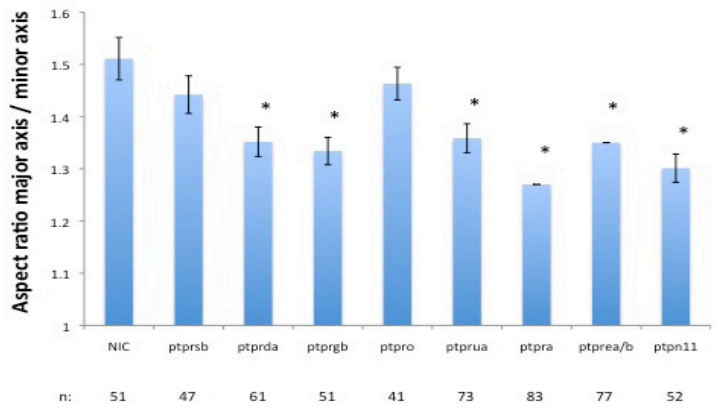
B
Aspect ratio major axis / minor axis
1.6
1.5
1.4
1.3
1.2
1.1
1
NIC
ptprsb
ptprda
ptprgb
ptpro
ptprua
ptpra
ptprea/b
ptpn11
n: 51 47 61 51 41 73 83 77 52

ptprua, and *ptpn11* morphants a strikingly similar pattern. The Cell Roses show a randomization of cell orientations as well as a clear loss of cell elongation indicated by a blue shift in the color code in comparison to the wild-type (Fig. 4A). The quantitative comparison of cell elongation reaffirms this significant decrease (Fig. 4 A,B). Of note, while the role for *ptprua* and *ptpn11* in CE movements has already been established, to our knowledge, this is the first study to provide direct evidence for the loss of cell polarization in the presomitic mesoderm of *ptprua* and *ptpn11* morphants.

Targeting ***ptprsb*** did not reveal a significant cell elongation defect in *ptprsb* knockdown embryos (Fig. 4 A,B). The Cell Roses showed a very slight randomization in the distribution of the polarization angles, yet a clear preference for the polarization angles in the mediolateral direction remained showing no significant difference to the positive controls (Fig. 4A). We conclude that the shortened body axis which is apparent at 72 hpf in *ptprsb* knockdown embryos is unlikely to be caused by defective CE movements.

Knockdown of ***ptprda*** caused a statistically significant difference in cell elongation (Fig. 4 A,B). Moreover, the Cell Rose showed a significant difference in the distribution of the polarization angles, demonstrated by a clear randomization, reminiscent of the pattern seen upon knockdown of PTPs known to play a role in CE movements (Fig. 4A). These results are consistent with a role for *ptprda* in CE movements.

Injection of **Ptpro**-specific MOs did not result in a statistically significant loss of cell elongation (Fig. 4 A,B). However, the Cell Rose showed a statistically significant randomization in the distribution of the polarization angles (Fig. 4A). This retaining of the cell elongation along with some randomization of the polarization angles is also indicated as red and brown areas on the cell rose (Fig. 4A). Given the retaining of cell elongation and the lower randomization of the polarization angles in comparison to the positive controls, we conclude that the shortened body axis which is apparent at 72 hpf upon knockdown of *ptpro* is unlikely to be caused by defective CE movements.

We found that knocking down ***ptprgb*** resulted in a significant loss of cell elongation (Fig. 4 A,B). Additionally, the cell rose showed a significant difference in the distribution of the polarization angles, yet a clear preference of direction was apparent, albeit deviating from the mediolateral direction (Fig. 4A). We conclude that the shortened body axis, which was apparent at 72 hpf in *ptprgb* knockdown embryos was more likely to be caused by mechanisms other than defective CE movements, because *bona fide* CE defects are characterized not only by defective cell elongation, but also by randomized distribution of the polarization angles.

Discussion

Identification of a putative effector of CE movements

We have performed a knockdown screen of the family of classical protein-tyrosine phosphatases. To our knowledge, this is the first time a MO- screen has been perfomed of an entire family of proteins. Our main goal was to identify PTPs with a role in CE movements. The workflow of the screen was subdivided into two main parts: morphological analysis and analysis of CE cell movements. 48 genes, which included seven PTPs with a known role in CE cell movements (*ptpra*, *ptprea*, *ptpreb*, *ptpn11*, *ptprua, ptpn13* and *ptpn20*), were systematically knocked down during zebrafish development and four genes with previously unknown function in zebrafish development were selected based on morphological parameters. Further analysis using *in situ* hybridization with known markers for CE movements and confocal microscopy-based cell polarity measurements, narrowed the number of putative hits to one *bona fide* novel PTP that acts in CE cell movements. For the other three hits from the morphological analysis, a different mechanism seems to underlie the observed phenotypes.

Evaluation of the screen

The MO screen described here has its pitfalls. One obvious problem is that the phenotype, which is considered positive in the morphological analysis, i.e. shorter body axis, is a known non-specific MO-induced artefact [32]. We used several controls to prevent false positives: (1) we never injected more than 5 ng MO and in general used the lowest amount which generates a phenotype [31]; (2) we injected a second sequence-independent MO to confirm the phenotype, which is generally established as the standard to assess specificity of MOs; (3) we coinjected both MOs with a p53-specific MO to establish that the observed defects were not due to a mere non-specific p53-dependent DNA-damage response [34]. A draw-back of the first control is that since we are using the lowest concentration of MO possible, it is not unlikely that the phenotype analyzed is a hypomorph and hence, we may miss MO-induced phenotypes (false negatives). In particular the genes for which only one of the MOs induced a phenotype are candidate false negatives.

Lack of functional redundancy between ptprsb, ptprda and ptprgb and their ohnologs

As mentioned above, there is functional redundancy between *ptprea* and *ptpreb*. Both genes need to be knocked down for a phenotype to become apparent. For *ptprsa/ptprsb*, *ptprda/ptprdb* and *ptprga/ptprgb* this is clearly not the case, indicating a functional divergence between these ohnologs. Moreover, for *ptprsa*, *ptprdb* and *ptprga* both MOs did not induce a phenotype, indicating that it

is unlikely that these genes have an essential function in early development. Apparently, the functions of these ohnologs have diverged.

The ohnologs *ptprsa/ptprsb* and *ptprga/ptprgb* have very similar expression patterns, especially during early development [17]. Interestingly, the expression patterns of *ptprda* and *ptprdb* differ greatly. While ptprda is maternally contributed and is expressed ubiquitously at the start of gastrulation, *ptprdb* seems not to be maternally contributed or expressed at the start of gastrulation [17]. This is consistent with a role for *ptprda* in early development. The functional divergence between *ptprda* and *ptprdb* may be explained by the difference in expression patterns, whereas *ptprsa/b* and *ptprga/b* presumably have different functions.

It should be noted for *ptprsa/ptprsb* and *ptprga/ptprgb* which show a similar expression pattern, that this screen did not include tests for partial redundancy between these gene couples, in that we did not include coinjection of MOs targeting both ohnologs. It is possible that the loss of *ptprsa* or *ptprga* was compensated by *ptprsb* or *ptprgb*, respectively, but not *vice versa*. It would be interesting to explore these possibilities.

Evolutionary conservation of PTP function

Gene functions of orthologs in distantly related species are often conserved. Here we compare the developmental defects in zebrafish morphants to the corresponding mouse knockout phenotypes.

Ptprsb is the ortholog of Ptprs in the mouse and it encodes a classical type IIb subfamily receptor-like PTP [17, 23]. *Ptprsb* knockdown in zebrafish caused small heads and eyes, and a severe cardiac edema. The *Ptprs* knock-out mouse displays early developmental defects, particularly in the nervous system [37]. These mice also display retarded growth, increased neonatal mortality, hyposmia, hypofecundity, and showed a decrease in overall brain size [38]. We conclude that zebrafish Ptprsb and mouse Ptprs have similar functions in early development.

Ptprda is a classical type IIb subfamily receptor-like PTP, the ortholog of mouse Ptprd [17, 39]. Knockdown of *ptprda* generated zebrafish embryos with only slight heart edema and bent tails. Like *Ptprs*, *Ptprd* has been shown to have an early developmental function in nervous system development in mouse [37]. Later phenotypes include semi-lethality due to insufficient food intake and learning impairment [40]. The zebrafish ptprda knockdown and mouse ptprd knockout are consistent, but because the mouse knock-outs predominantly display late defects and we analyzed only early developmental defects in zebrafish embryos, the phenotypes are hard to compare definitively.

Zebrafish **Ptpro**, ortholog of mouse Ptpro, encodes a classical type III subfamily receptor-like PTP, characterized by a cytoplasmic region with a single PTP domain and an extracellular region comprising 8 Fibronectin type III repeats [17, 41, 42]. The Zebrafish *ptpro* morphants had smaller heads and heart edemas. Two distinct *ptpro*-deficient mouse models have been generated. The first Ptpro knock-out model displays an altered podocyte structure associated with hypertension and low glomerular filtration rate [43]. The second Ptpro knock-out displays defects in the development and function of the sensory nervous system [44]. Given the discrepancy in developmental defects in the two mouse knock-out models, it remains to be determined definitively whether zebrafish and mouse Ptpro have orthologous functions.

Ptprgb is the ortholog of Ptprg, a classical type V subfamily receptor-like PTP [17, 45]. MOs targeting *ptprgb* induced severe shortening of embryos, heart edemas and a slight hindbrain edema. Mouse Ptprg is expressed in pyramidal cells and sensory neurons in the nervous system. Ptprg knock-out mice develop normally and it appears that Ptprg is not required for normal development [46]. Apparently, Ptprgb is not dispensable for normal embryonic development in zebrafish and hence the function of Ptprgb differs from mouse Ptprg.

Conclusion

We conclude that a MO screen on an entire gene family with 48 members is feasible in zebrafish. Next to the seven known PTPs with a role in CE cell movements, we have identified one additional PTP that is essential for normal gastrulation cell movements, Ptprda. It will be interesting to investigate how Ptprda affects gastrulation cell movements and whether it interacts with the signaling pathway that is well-known to regulate CE movements, the non-canonical Wnt pathway. In addition, it will be interesting to investigate cross-talk among all PTPs that have been identified to play a role in CE cell movements.

Materials and methods

Zebrafish maintenance and in situ hybridization

Zebrafish were kept and the embryos were staged as described before [47]. *In situ* hybridizations were done essentially as described [48] =- using probes specific for *krox20* and *myod*.

Morpholinos, in vitro transcription of mRNA and injection

Antisense splice site MOs were designed to target one or two exons upstream of the phosphatase catalytic site and manufactured by GeneTools (Pilo-

math, OR, USA). Using the mMessage mMachine kit (Ambion), we synthesized 5' sense mRNA encoding membrane citrine (a YFP variant with a C-terminal fusion of the Ras membrane localization sequence [CAAX]). The embryos were injected at one cell stage.

Confocal microscopy, positioning and analysis

To visualize the cell shape in the presomitic mesoderm, membrane citrine expressing live embryos were mounted in 0.75% soft agarose at the dorsal side in glass bottomed petri dishes. Using SP2 Leica Confocal microscope the presomitic mesoderm was imaged using a 40 X oil objective. 2-D images were acquired during the 2 to 3 somite stage 100 μm posterior to the developing somites in the paraxial mesoderm, lateral to the notochord. Automated segmentation of cell membranes using Cell Outliner and Cell rose based analysis was performed as described before in Chapter 5 of this thesis.

References

1. Hunter, T., *Protein kinases and phosphatases: the yin and yang of protein phosphorylation and signaling.* Cell, 1995. **80**(2): p. 225-36.

2. van der Geer, P., T. Hunter, and R.A. Lindberg, *Receptor protein-tyrosine kinases and their signal transduction pathways.* Annu Rev Cell Biol, 1994. **10**: p. 251-337.

3. Van Vactor, D., A.M. O'Reilly, and B.G. Neel, *Genetic analysis of protein tyrosine phosphatases.* Curr Opin Genet Dev, 1998. **8**(1): p. 112-26.

4. den Hertog, J., *Protein-tyrosine phosphatases in development.* Mech Dev, 1999. **85**(1-2): p. 3-14.

5. Alonso, A., et al., *Protein tyrosine phosphatases in the human genome.* Cell, 2004. **117**(6): p. 699-711.

6. Hendriks, W.J., et al., *Protein tyrosine phosphatases: functional inferences from mouse models and human diseases.* FEBS J, 2008. **275**(5): p. 816-30.

7. LaForgia, S., et al., *Receptor protein-tyrosine phosphatase gamma is a candidate tumor suppressor gene at human chromosome region 3p21.* Proc Natl Acad Sci U S A, 1991. **88**(11): p. 5036-40.

8. Tartaglia, M., et al., *Mutations in PTPN11, encoding the protein tyrosine phosphatase SHP-2, cause Noonan syndrome.* Nat Genet, 2001. **29**(4):

p. 465-8.

9. Wang, Z., et al., *Mutational analysis of the tyrosine phosphatome in colorectal cancers.* Science, 2004. **304**(5674): p. 1164-6.

10. Roszko, I., A. Sawada, and L. Solnica-Krezel, *Regulation of convergence and extension movements during vertebrate gastrulation by the Wnt/PCP pathway.* Semin Cell Dev Biol, 2009. **20**(8): p. 986-97.

11. Warga, R.M. and C.B. Kimmel, *Cell movements during epiboly and gastrulation in zebrafish.* Development, 1990. **108**(4): p. 569-80.

12. Heisenberg, C.P., et al., *Silberblick/Wnt11 mediates convergent extension movements during zebrafish gastrulation.* Nature, 2000. **405**(6782): p. 76-81.

13. Jessen, J.R., et al., *Zebrafish trilobite identifies new roles for Strabismus in gastrulation and neuronal movements.* Nat Cell Biol, 2002. **4**(8): p. 610-5.

14. Sepich, D.S., et al., *Role of the zebrafish trilobite locus in gastrulation movements of convergence and extension.* Genesis, 2000. **27**(4): p. 159-73.

15. Topczewski, J., et al., *The zebrafish glypican knypek controls cell polarity during gastrulation movements of convergent extension.* Dev Cell, 2001. **1**(2): p. 251-64.

16. Solnica-Krezel, L., *Gastrulation in zebrafish -- all just about adhesion?* Curr Opin Genet Dev, 2006. **16**(4): p. 433-41.

17. van Eekelen, M., et al., *Identification and expression of the family of classical protein-tyrosine phosphatases in zebrafish.* PLoS One, 2010. **5**(9): p. e12573.

18. Jopling, C., D. van Geemen, and J. den Hertog, *Shp2 knockdown and Noonan/LEOPARD mutant Shp2-induced gastrulation defects.* PLoS Genet, 2007. **3**(12): p. e225.

19. van Eekelen, M., et al., *RPTPalpha and PTPepsilon signaling via Fyn/Yes and RhoA is essential for zebrafish convergence and extension cell movements during gastrulation.* Dev Biol, 2010. **340**(2): p. 626-39.

20. Aerne, B. and D. Ish-Horowicz, *Receptor tyrosine phosphatase psi is required for Delta/Notch signalling and cyclic gene expression in the presomitic mesoderm.* Development, 2004. **131**(14): p. 3391-9.

21. van eekelen, M., runtuwene, V., masselink, W., den Hertog, J., *Pairwise regulation of convergence and extension cell movements by four phosphatases via RhoA.* submitted.

22. Flicek, P., et al., *Ensembl's 10th year.* Nucleic Acids Res, 2010. **38**(Database issue): p. D557-62.

23. Pulido, R., et al., *The LAR/PTP delta/PTP sigma subfamily of transmembrane protein-tyrosine-phosphatases: multiple human LAR, PTP delta, and PTP sigma isoforms are expressed in a tissue-specific manner and associate with the LAR-interacting protein LIP.1.* Proc Natl Acad Sci U S A, 1995. **92**(25): p. 11686-90.

24. Saunders, A.E. and P. Johnson, *Modulation of immune cell signalling by the leukocyte common tyrosine phosphatase, CD45.* Cell Signal, 2010. **22**(3): p. 339-48.

25. Aguiar, R.C., et al., *PTPROt: an alternatively spliced and developmentally regulated B-lymphoid phosphatase that promotes G0/G1 arrest.* Blood, 1999. **94**(7): p. 2403-13.

26. Elson, A. and P. Leder, *Protein-tyrosine phosphatase epsilon. An isoform specifically expressed in mouse mammary tumors initiated by v-Ha-ras OR neu.* J Biol Chem, 1995. **270**(44): p. 26116-22.

27. Amoui, M., et al., *Expression of a structurally unique osteoclastic protein-tyrosine phosphatase is driven by an alternative intronic, cell type-specific promoter.* J Biol Chem, 2003. **278**(45): p. 44273-80.

28. Imai, Y. and W.S. Talbot, *Morpholino phenocopies of the bmp2b/swirl and bmp7/snailhouse mutations.* Genesis, 2001. **30**(3): p. 160-3.

29. Braat, A.K., et al., *A zebrafish vasa morphant abolishes vasa protein but does not affect the establishment of the germline.* Genesis, 2001. **30**(3): p. 183-5.

30. Lele, Z., J. Bakkers, and M. Hammerschmidt, *Morpholino phenocopies of the swirl, snailhouse, somitabun, minifin, silberblick, and pipetail mutations.* Genesis, 2001. **30**(3): p. 190-4.

31. Ekker, S.C. and J.D. Larson, *Morphant technology in model developmental systems.* Genesis, 2001. **30**(3): p. 89-93.

32. Heasman, J., *Morpholino oligos: making sense of antisense?* Dev Biol, 2002. **243**(2): p. 209-14.

33. Ekker, S.C., *Nonconventional antisense in zebrafish for functional genomics applications.* Methods Cell Biol, 2004. **77**: p. 121-36.

34. Robu, M.E., et al., *p53 activation by knockdown technologies.* PLoS Genet, 2007. **3**(5): p. e78.

35. Li, C., et al., *An essential role for DYF-11/MIP-T3 in assembling functional intraflagellar transport complexes.* PLoS Genet, 2008. **4**(3): p. e1000044.

36. Runtuwene, V., et al., *Noonan syndrome gain-of-function mutations in NRAS cause zebrafish gastrulation defects.* Dis Model Mech, 2011. **4**(3): p. 393-9.

37. Chagnon, M.J., N. Uetani, and M.L. Tremblay, *Functional significance of the LAR receptor protein tyrosine phosphatase family in development and diseases.* Biochem Cell Biol, 2004. **82**(6): p. 664-75.

38. Elchebly, M., et al., *Neuroendocrine dysplasia in mice lacking protein tyrosine phosphatase sigma.* Nat Genet, 1999. **21**(3): p. 330-3.

39. Pulido, R., et al., *Molecular characterization of the human transmembrane protein-tyrosine phosphatase delta. Evidence for tissue-specific expression of alternative human transmembrane protein-tyrosine phosphatase delta isoforms.* J Biol Chem, 1995. **270**(12): p. 6722-8.

40. Uetani, N., et al., *Impaired learning with enhanced hippocampal long-term potentiation in PTPdelta-deficient mice.* EMBO J, 2000. **19**(12): p. 2775-85.

41. Seimiya, H., et al., *Cloning, expression and chromosomal localization of a novel gene for protein tyrosine phosphatase (PTP-U2) induced by various differentiation-inducing agents.* Oncogene, 1995. **10**(9): p. 1731-8.

42. Wiggins, R.C., et al., *Molecular cloning of cDNAs encoding human GLEPP1, a membrane protein tyrosine phosphatase: characterization of the GLEPP1 protein distribution in human kidney and assignment of the GLEPP1 gene to human chromosome 12p12-p13.* Genomics, 1995. **27**(1): p. 174-81.

43. Wharram, B.L., et al., *Altered podocyte structure in GLEPP1 (Ptpro)-deficient mice associated with hypertension and low glomerular filtration rate.* J Clin Invest, 2000. **106**(10): p. 1281-90.

44. Gonzalez-Brito, M.R. and J.L. Bixby, *Protein tyrosine phosphatase receptor type O regulates development and function of the sensory nervous system.* Mol Cell Neurosci, 2009. **42**(4): p. 458-65.

45. Barnea, G., et al., *Identification of a carbonic anhydrase-like domain in the extracellular region of RPTP gamma defines a new subfamily of receptor tyrosine phosphatases.* Mol Cell Biol, 1993. **13**(3): p. 1497-506.

46. Lamprianou, S., et al., *Receptor protein tyrosine phosphatase gamma is a marker for pyramidal cells and sensory neurons in the nervous system and is not necessary for normal development.* Mol Cell Biol, 2006. **26**(13): p. 5106-19.

47. Westerfield, *The zebrafish book*. 1995: University of Oregon press, Eugene, Oregon.

48. Thisse, C., et al., *Structure of the zebrafish snail1 gene and its expression in wild-type, spadetail and no tail mutant embryos.* Development, 1993. **119**(4): p. 1203-15.